

## Landslide detection and inventory by integrating LiDAR data in a GIS environment

**Abstract** In this work, a simple methodology is presented for processing high-resolution topographical data over wide areas. It is based on digital elevation model of differences (DEMoD) among high-resolution digital models (HRDEM) produced from light-detection and ranging (LiDAR) data. Because these qualitative approaches based on HRDEMs can be affected by errors related to misalignment between different passes of the airborne sensor and errors in classifying points, a simplified strategy was undertaken for their semi-automatic correction and supervision for analyzing geomorphological changes. Besides, it became possible to detect, delineate, and classify a total of 47 natural landslides and 50 slope-cut failures over an area of 234km<sup>2</sup> on the basis of the analysis of the LiDAR products (DEMs and DEMoD) and the orthophotography imagery inspection integrated in a geographical information system (GIS). Most of the displacements detected were probably generated during the winter of 2009–2010 when a new record of cumulative rainfall was reached. The displacement rate of these movements cannot be known with precision, but the minimum velocity that can be obtained is 0.3m/year regarding the period between the two data acquisitions carried out in November 2008 and July 2010. On the other hand, a comparison was made of the existing susceptibility maps with respect to this new inventory, which indicated greater landslide frequency in areas of moderate susceptibility levels. The influence of treating inventories at different temporal scales is discussed.

**Keywords** LiDAR data · GIS · DEMoD · Betic Cordillera · Spain

### Introduction

In the framework of the calculation of total risk due to landslides, the well-known definition of Varnes (1984): “the expected number of lives lost, persons injured, damage to property and disruption of economic activity due to a particular damaging phenomenon for a given area and reference period” is frequently applied. This implies that the spatial and temporal occurrence probability of one specific event must be quantified (Brabb 1984; van Westen et al. 2006), and for that, the first and most important step is to get the inventory as another layer of the input data such as is underlined in the literature (Soeters and van Westen 1996; Cascini et al. 2005; van Westen et al. 2008; Guzzetti et al. 2012). A description of the basic data sets required for susceptibility and hazard assessments can be found in Fell et al. (2008) and in van Westen et al. (2008), as well as they present a summary of techniques for the collection of landslide information at different scales. The recent work of Corominas et al. (2014) extends these recommendations to quantitative risk analysis (QRA) the recent work of Corominas et al. (2014) can be consulted. Nevertheless, when inventory maps and databases of landslides are made appear different problems (van Westen et al. 2008, 2006) which also make it difficult to standardize the methods for deal with the risk assessment in an objective and reproducible way (Galli et al. 2008; Guzzetti et al. 2012). They

are basically due to the diversity of types of landslides, mechanisms of initiation or reactivation, or changes in the preparatory factors, as well as the important lack of historical data on dating and characteristics of events happening (Ibsen and Brunsten 1996) that are only recorded in a timely manner after events that cause substantial damage or when they are selected as research objects. As a consequence, the existing information is often incomplete, outdated, and lacks good quality (Cascini 2008; Corominas et al. 2014; Van Den Eeckhaut and Hervás 2012; van Westen et al. 2008). This matter is exacerbated when dealing with quantifying the frequency of occurrence or analyzing the landslide activity and development (Chacón et al. 2010), which involves generating big amounts of information on this phenomenon with minimum effort while saving time, mainly working in mapping from local to minor scales (more than 10 km<sup>2</sup>) (Cascini 2008; Corominas et al. 2014). A review of several studies of inventory with production time (from several months to several years) can be found in Guzzetti et al. (2012). Despite these problems, in the last decade, there have been efforts to draft guidelines for applying different methodologies and techniques to the zoning of the main components of risk (inventory, susceptibility, hazard, and vulnerability) depending on the scale and level of detail required by the type of work (Cascini 2008; Corominas et al. 2014; Fell et al. 2008).

Unlike conventional techniques, those based in remote sensing and altimetry constitute fundamental tools for rapid and precise mapping of geomorphological features (Hervás et al. 2003; Baum et al. 2005; Ardizzone et al. 2007; Fernández et al. 2008; Prokešová et al. 2010; Guzzetti et al. 2012; Daehne and Corsini 2013; Roering et al. 2013), allowing inaccessible areas to be covered and enabling the preparation of more complete inventories in a semi-automatic way (Guzzetti et al. 2012; Jaboyedoff et al. 2012). The laser altimeter based on light-detection and ranging (LiDAR), airborne or terrestrial, has evolved in the last 15 years (Haneberg et al. 2009; Derron and Jaboyedoff 2010), enabling to the creation of high-resolution and precise digital elevation models with HRDEM (McKean and Roering 2004; Glenn et al. 2006; Kasai et al. 2009). These models have been used to evaluate land changes with greater precision, often integrating DEMs from other techniques such as photogrammetry, in different research strategies (Dewitte et al. 2008; Marsella et al. 2009; Fernández et al. 2011, 2013) or terrestrial laser scanner (Jaboyedoff et al. 2012; Wang et al. 2013). Most of these works involve working with small areas (a few km<sup>2</sup> or tens of km<sup>2</sup>) in which the generation and edition of DEMs are not a too long time-consuming process.

In view of these advantages, the aim of this work is to develop a feasible methodology integrating the LiDAR processing in a geographical information system (GIS) environment to collect landslide features and data periodically to be used in the assessment of the total risk and their components (Carrara et al. 1999; Chacón et al. 2006a, b) in relatively large areas (hundreds of km<sup>2</sup>). In a nutshell, to highlight and cartography terrain changes, the methodology was based in Digital Elevation Model of Differences (DEMoD) (Daehne and Corsini 2013)

supported by the visual inspection of the underlying orthophoto imagery as an attempt to easily produce inventories in an effective and regular manner. The methodology was applied in an area of 234 km<sup>2</sup> using LiDAR data corresponding to the dates November 2008 and July 2010, which includes only two seasonal cycles, the second one (2009–2010) characterized by critical rainfall periods resulting in damages for infrastructures and private properties. These inventories of relative short periods or covering few seasonal cycles can be classified as seasonal inventories. Finally, the resulting inventory of short time interval compared to the input inventory used to generate the existing susceptibility model in the study area is not considered enough complete to carry out a real validation of such a model. Nevertheless, to this goal, the new inventory was regarded as a preliminary data and its spatial distribution taking into account the different lithology as well as the existing zoning susceptibility (potential for landslides) based on historical geomorphological inventory of higher temporal extension (Guzzetti et al. 2012) was analyzed and discussed.

### Characteristics of the study area

The present study lies in southern Spain and extends 234 km<sup>2</sup> throughout the Guadalfeo basin, which can be considered a

relatively large area to be studied at medium or local-regional scales (1:10.000–1:100.000) (Cascini 2008; Fell et al. 2008) and geologically located in the Internal Zones of the Betic Cordillera. This is composed primarily of metamorphic rocks of both the Nevado-Filabride and the Alpujarride Complexes, which cover an area of steep slopes resulting from alpine orogeny and crossed by deep valleys; in addition, there are post-tectonic Neogene and Quaternary deposits located in the topographically lowest part with gentle slopes (Fig. 1). In the Nevado-Filabride Complex, dark schists and feldspathic mica schists are widespread, while the Alpujarride Complex is composed of Triassic calcareous schists together with marbles, phyllites, and quartzites (Gómez-Pugnaire et al. 2004). The Neogene lithology is composed of marls and silts covered with conglomerates, colluvial deposits in the lower part of a slope, and alluvial fill transported throughout the watershed.

The different combinations of lithology and type of relief are associated with the expected landslides types (Chacón et al. 2010). In this area, the translational and rotational slides, debris flows, and rockfalls can be found, some of them related to the mechanical properties of the lithology sited between tectonic boundaries, for instance, the existing landsliding activity in the surrounding of

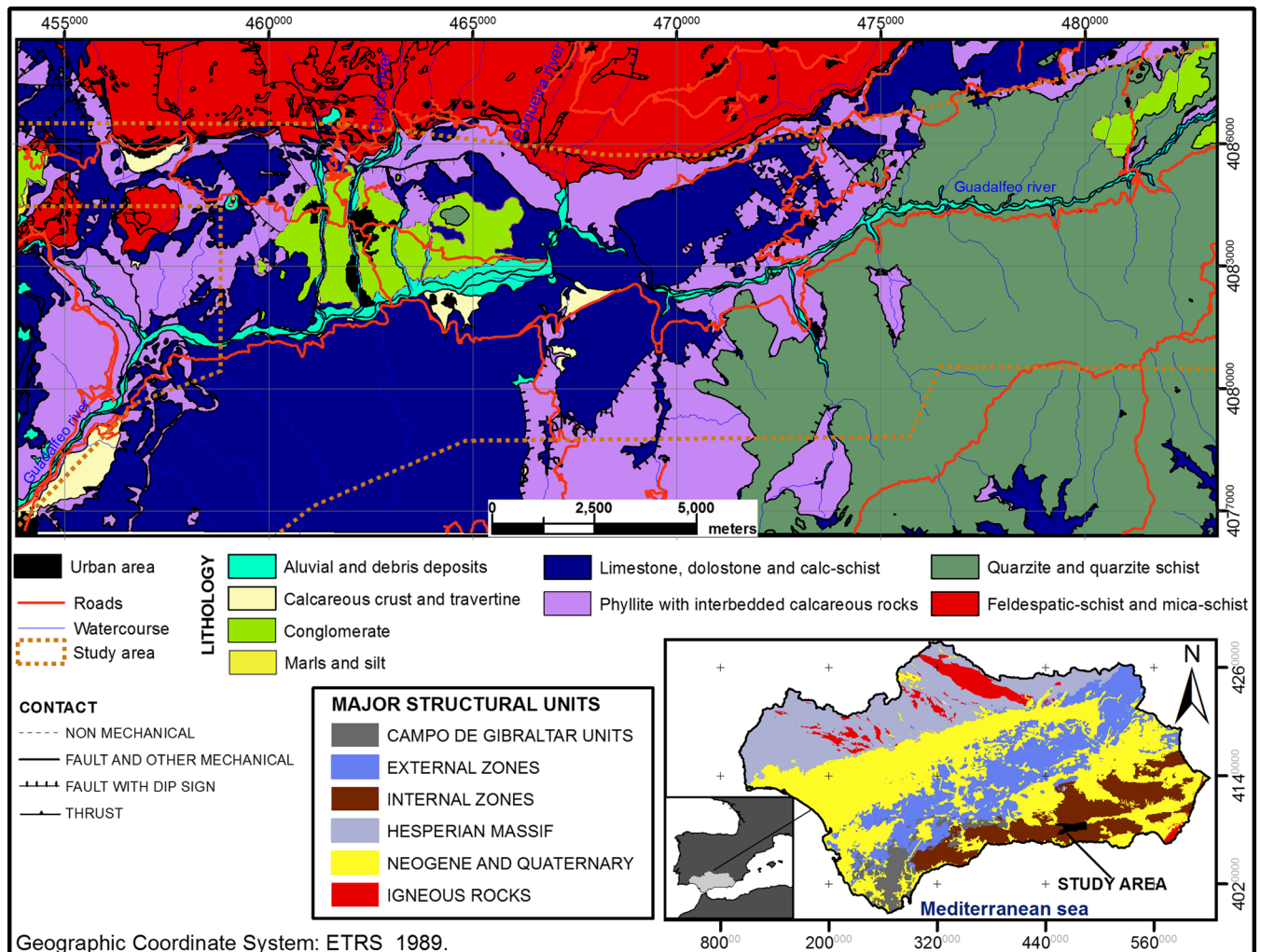


Fig. 1 Geographical location of the study area on the lithological and structural map of the Betic Cordillera and location and major structural units (bottom map)

the contact between phyllites and schists, or through the tectonic contact between coarse clastic deposits (silts, sands, and conglomerates) and the Alpujarride Complex (Chacón et al. 2006a, b). Landsliding have been investigated in this area for several decades as a generalized and hazardous denudation process, including some inventories distributed in various adjacent areas: the environs of the Guadalfeo river (Fernández et al. 2009; Jiménez-Perálvarez et al. 2011); the Ízbor river basin (El Hamdouni et al. 2008); and Sierra de La Contraviesa and Sierra de Los Guájares (Fernández et al. 2003; Irigaray et al. 2007). These inventories are made through photointerpretation techniques with the aid of field work, including the size and type of landslide, stage of development, and the activity and lithology of each area. In addition, with these inventories used as entry data together with other geomorphological variables and the lithology, the susceptibility map was constructed from the determining factors, with the use of a GIS Matrix Methodology (GMM) (Irigaray et al. 1999; Fernández et al. 2003; Irigaray et al. 2007), recently optimized (Jiménez-Perálvarez et al. 2011). Figure 2 illustrated the landslide-susceptibility zoning established for the study area in the environs of the Sierra de La Contraviesa and published in the natural hazards atlas of the Granada province (DIPGRA/IGME 2007). The percentage of the corresponding area for each final susceptibility class regarding the investigated extent are 2.87 % (very low), 14.21 % (low), 61.15 % (moderate), 21.66 % (high), and 0.11 % (very high). The validation and quality of this map was assessed by applying the degree of fit (DOF) (Jimenez-Peralvarez et al. 2009) and using a different inventory than that used for the susceptibility assessment. The DOF is defined as follows:

$$DOF_i = \frac{m_i/t_i}{\sum m_i/t_i}$$

where  $m_i$  is the area occupied by the source areas of the landslides at each susceptibility level or class  $i$ , and  $t_i$  is the total area covered by that susceptibility class. This DOF represent the percentage of mobilized area located in each of those classes. For the present susceptibility zoning, the DOF is lower (<7 %) in the

low and very low classes, and therefore showing a relative error, while the value of the DOF increases with higher classes (relative accuracy) (Jimenez-Peralvarez et al. 2009).

The predominant Mediterranean climate of the study area is characterized by a varied rainfall pattern with long-dry summers during which violent storms happen and wet winters. Nonetheless, some historic anomalies have been detected, as occurred in the winter 1996–1997 when the rainfall was more than double the average, resulting in multiple damages to the road network of this area (Irigaray et al. 2000). And more recently, in the wet period of the winter 2009–2010 covered by the time window between the data used in the present work, another record was reached as revealed by the accumulative rainfall registered in pluviometric stations spread over the Guadalfeo basin. The report of AEMET (2010) states that in general, for the hydrological year 2009–2010 the cumulative precipitation exceeded 50 % of the average cumulative precipitation for a typical hydrological year in Spain. On the other hand, taking into account the most representative stations in the area, the cumulative precipitation reached 247 % (Torvizcón station) and 221 % (Órgiva station) with respect to the average in the wet months from October 2009 to March 2010, corresponding to quantities measured of 485 and 782 mm, respectively (Irigaray and Palenzuela 2013; Palenzuela et al. 2013). This precipitation triggered numerous floods, landslides, and heavy erosion, damaging private property as well as civil infrastructures.

#### Materials and data

The two LiDAR databases were compiled by flights on two dates, November 2008 and July 2010 including the wet cycle of the winter 2009–2010 when atypical rainfall took place, as described above.

From each database, 75 common tiles (150 in total) were selected  $2 \times 2$  km, and the mean density of the data was calculated, giving values of 0.31 and 0.34 points/m<sup>2</sup>, for the first and second flight, respectively. In addition, the spacing between points averaged 1.20 m for the first flight and 1.08 for the second. Following these parameters, the average number of points per part in the first flight reached 2,721,214 million points and 3,318,737 million for the second.

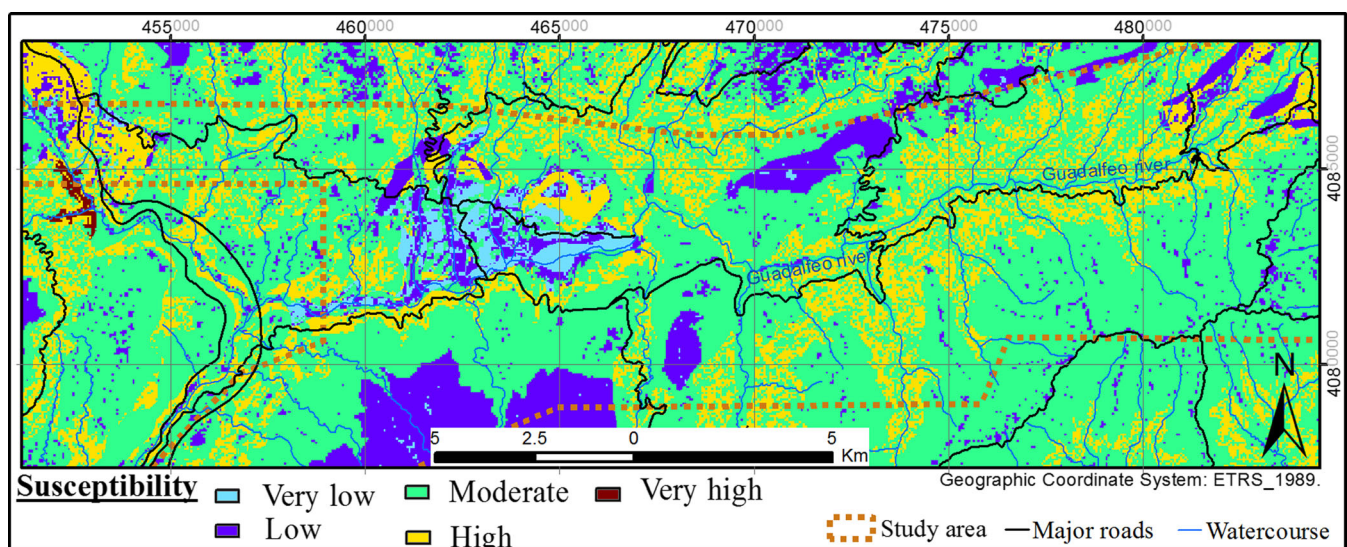


Fig. 2 Susceptibility zoning in the study area



The data were gathered with the airborne laser scanner 50 II (Leica 2006) from an average height of 2000 m, which resulted in predicted measurement errors in distances of less than 0.30 m, and an illuminated footprint of 0.32 m<sup>2</sup> (Leica 2006). These errors are acceptable within the scope of geomorphological studies (Tarolli et al. 2012) at a level of detail of detecting and quantifying terrain morphology (Singhroy and Molch 2004) (small scars, heads of ravines, channel, sandbars, etc.) from contour maps with intervals less than a meter (Prokop and Panholzer 2009) or HRDEMs. This technology enables the production of HRDEMs, from which precise maps are drawn and directly georeferenced, avoiding certain typical human errors in the field work due to reduced visibility when the best vantage points cannot be reached to delineate the landslides and where subjectivity appears in decision making based on the judgment of the expert (Baum et al. 2005; Ardizzone et al. 2007), or simply for not having access to all the parts of the study area. Other errors that add to the measurement involve the precision of the coordinates of the position caused by the differential geographical positioning system (DGPS), as well as errors in the orientation determined by the inertial navigation system (INS). This provokes centimetric errors in the points on the XY plane, the effect being more pronounced in the elevation coordinate (Z) ( $\approx 5$  cm). However, in areas of steep slopes and forests, the dispersion of the beam and the illumination footprint are multiplied by tens to hundreds of times these values, depending on the Z coordinate of the deviation in the position on the XY plane, and thus some points can vary several meters in the least favorable areas, although the error can be less than with some conventional methodologies of photogrammetry at similar scales (McKean and Roering 2004; Baum et al. 2005).

All these errors resulted in translations and rotations of the set of points with respect to their correct position and orientation and consequently in the misalignment between the passes of the LiDAR sensor seen as a slide-lap effect in the border areas between

these bands (Ardizzone et al. 2007). As the raw data or those in standard LAS format were divided by the flight agency into two square parts of 2×2 km in order to reduce the computational cost in the post-processing tasks, some minimal maladjustments were detected also in the parts near the adjacent edges after the data were adjusted by the present methodology due to the loss of lateral consistency. Finally, apart from these errors inherent to the data-gathering instruments and the georeferencing, there are non-system errors resulting in the mistaken classification of the points measured in the objects by different methods.

### Methodology

The methodology represented schematically in the flow diagram in Fig. 3 can be divided into the following steps where the two types of DEMs are generated from the raw data for their processing, digital terrain model (DTM) containing the bare earth surface and digital surface model (DSM) that also includes all the other elements on the ground as follows:

- Classification of the LiDAR data.
- Interpolation of the LiDAR data.
- First comparison of the DTMs and adjustment of the alignment.
- Comparison of the DTMs of the adjusted data.
- Comparison of the DSMs, determination of the combined DEMoD, and digitalization of features.

It bears emphasizing that many of the processes are applied directly in GIS (ESRI 2013) in order to integrate the new database with other layers of georeferenced information later used in geomorphological research or in other types of studies, projecting each in the European Terrestrial Reference System 1989 (ETRS89) in conjunction with the ellipsoid height. In addition,

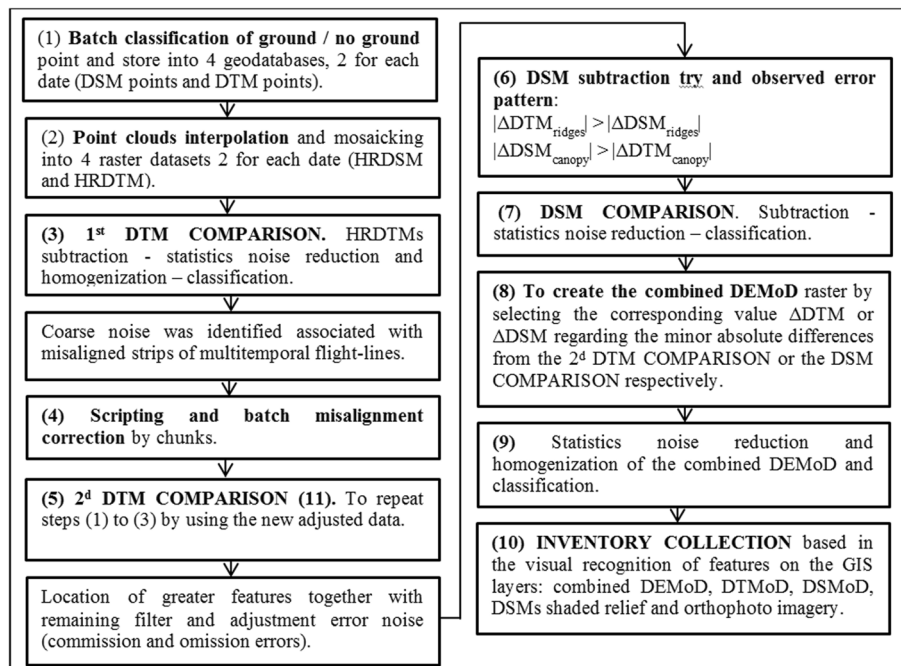


Fig. 3 Work flow sketch



some models of tools and scripts were created for automating certain iterative tasks that consumed greater work time.

### LIDAR classification

Despite that the LiDAR data allow the preliminary assignment of points to different types of objects (terrain, low vegetation, trees, buildings, etc.) making use of the order of returning beams reflected (up to 4 rebounds with the Leica50 II scanner), which constitutes an advantage in wooded and urban areas where even previously unknown land forms are revealed (Roering et al. 2013), a correct classification and assignation of points to the terrain cannot always be achieved. For example, in woods with a dense canopy or constructions, it is common for all the rebounds to come from objects higher than the ground, so that the last rebound that is assigned to the terrain would be misclassified in these cases. Therefore, it is recommended to use filtered added mathematics that improve this classification between ground points and non-ground points (Axelsson 2000; Zhang et al. 2003; Evans and Hudak 2007; Meng et al. 2010). In this way, in this first stage, the data are classified by a filter commonly used for this type of progressive densification (Axelsson 2000) implemented in LAStools software (Isenburg 2013), being applicable to any type of surface (from mountainous and forested areas to flat urban zones). However, this filtering ends up beveling some abrupt areas and crests of terrain that need to be taken into account in order to analyze the results in successive stages of the processing. Currently, the improvement of the filtering algorithms to avoid this problem continue to be a challenge in the classification strategies of LiDAR data (Evans and Hudak 2007; Zhang et al. 2003), and as long as this is not perfected, its application can result in the omission of analysis areas where errors can be significant. The classified LAS files were then imported into four GIS geodatabases, two for each date (DSM points and DTM points) (Fig. 3 (1)).

### Interpolation

Once the points measured were classified, some trials were made to optimize the interpolation phase. First, different cell sizes were used to find the ones most suitable for the products created from the original data. For this, the points were converted to a raster format, assigning the value “No Data” to cells when there was no point projected over the domain of the corresponding pixel, and

the parameters of average density ( $\approx 1$  point per  $3 \text{ m}^2$ ) and average spacing between points ( $\approx 1.1 \text{ m}$ ) were taken into account.

Figure 4 shows three DSM rasters resulting from applying three different cell sizes. In the first trial, a size of 1 m (a value close to that of the spacing) produced a greater number of No Data values, which are shown as white “holes” and represent areas of insufficient data. In the case of the raster with a pixel size of 2 m, the number of No Data cells is almost the same as for the first case. Finally, with a cell size of 2.5 m, the number of No Data pixels diminished considerably, although the resolution or distribution of elevation data was less in the raster (1 value per  $6 \text{ m}^2$ ) than in the original points cloud (1 value per  $3 \text{ m}^2$ ). Therefore, this unit cell size was selected to produce the DSMs, since it can represent the interpolated values (predicted) with a resolution that best approximates that of the points cloud measured—that is, with minimum loss of original resolution in terms of density but without overexploiting the areas without data.

On the other hand, different interpolation methods were tested to select a faster and more efficient one that would be applicable to all the parts of the division of the scanned datasets, all of them based on well-known interpolators implemented in ArcGIS. The first one consisted of a combination of points to raster transformation and then the holes are closed by means of a geostatistical reclassification based in a matrix of  $3 \times 3 \text{ m}$  calculating the mean value in the central cell, also were applied two common types of kriging interpolators, these are, the simple and ordinary kriging with default parameters, and lastly, the inverse distance weighted (IDW) interpolation using 15 neighbors to calculate the predicted values.

To evaluate the results of the interpolation methods, two different approaches were applied: cross validation through an integrated tool in the GIS package and the residuals or variation in height of the point with respect to the raster model interpolated. The first approach evaluates the differences between the entire data set used to generate the model comparing the predicted values with the original ones. The latter was automated in a model of GIS tools and permits the selection of a random sample of the original points cloud and its direct comparison by the calculation of the residuals taking as a base the interpolated raster. This model calculates new columns with the vertical residuals ( $\Delta Z$ ) and its absolute values, introducing them into the same database that contains the test set. Optionally, the tool offers the possibility of

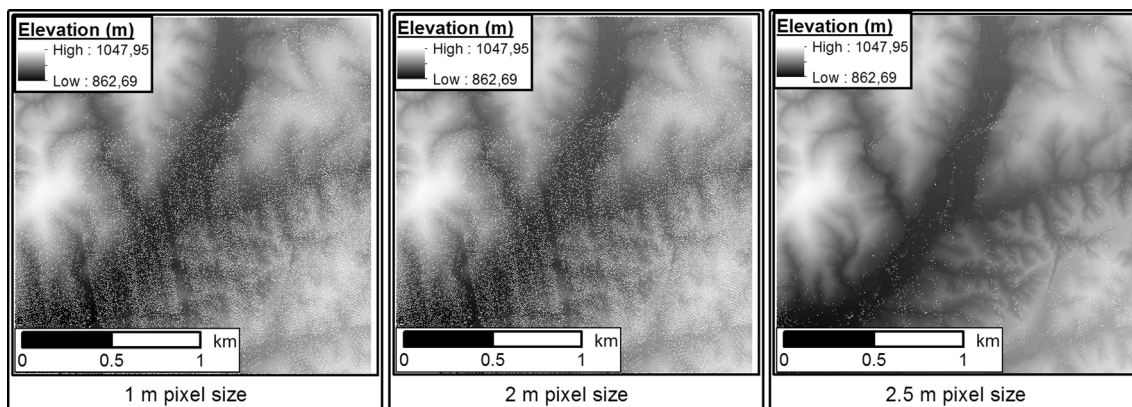


Fig. 4 No Data (holes) distribution converted point to DSM raster for different pixel sizes

directly representing the residual values on a color map on selecting any interpolation model from among those included in ArcMap. All of the interpolation strategies were carried out for the same training data set with a number of 2000 points selected at random and set at a minimum distance of 20 m apart.

The results are statistically summarized to be compared. The mean and standard deviation (SD) of the absolute value of the residuals are presented in Table 1, where it is shown that the IDW offers the best approximation. This suggests that the kriging model is not as good for representing the data distributed with patterns of a certain irregularity in which it is difficult to fit the parameters of the function to this trend. However, IDW is a rapid interpolator that can be applied to the data bases in a deterministic and understandable way, or can be easily reproduced through all the interpolated parts. As a consequence, the IDW interpolator is applied to all the parts (LiDAR data tiles) of the two geodatabases on each date that were afterwards pooled to generate each mosaic of DEMs. This resulted in four new raster datasets, one HRDSM and one HRDTM for each date by using the classified point clouds stored in the geodatabases (Fig. 3 (2)).

### First DTM comparison and alignment fit

This phase consists of the subtraction of the first DTM of the acquisition sequence (year 2008) to the last (year 2010). After this step, the noise of the results is reduced in order to isolate the changes in the terrain. For this, the DEMoD values were rounded to their nearest integers and then a statistical filter was applied for which a window of  $3 \times 3$  pixels was used to determine the most frequent discrete value assigned to each pixel, which produces a discrete preliminary classification that can be supervised visually in an easier way (Fig. 3 (3)), permitting the highlighted features to be delineated.

In this first comparison, the resulting DEMoD (in reality, it should be called DTMoD) reveals some of the common errors when acquiring and processing LiDAR data; on the one hand, the misalignment or poor fit between the sequential passes of the measuring sensor detected in border areas and on terrain parts of pronounced slopes, and on the other hand the erroneous classification of the data in rural zones and urbanized ones, and to a lesser degree in forested sectors where a great part of the vegetation was correctly eliminated (Fig. 5), according to the classification procedures described above.

The systematic error of misalignment can be partially corrected by an adjustment of the original data. In this particular case, a data base of ground control points (GCP) is not available, making it necessary to measure these points onsite (by GPS), with the substantial increase in time. This is added to the significantly high computational time and cost when such a volume of data is

treated. To overcome these limitations, the following procedure, which was considered appropriate for this type of study, was applied.

Initially, an individual alignment error was identified for only 1 year, revealing a major poor fit between the points scanned within the three adjacent parts (tiles with a total surface area of  $6 \times 2$  km) of the data belonging to the 2008 flight. This sample of data was taken to confirm the poor alignment for being a zone where greater differences were detected between the data of one or another year, following adjacent patterns in overlapping zones of several passes of the scan of the 2008 flight with a mean error of  $-0.53$  m and a SD of 1.07 m (Fig. 5a and b). On the contrary, the same area in the data from 2010 presented a lower mean error ( $-0.034$  and a SD of 0.58), which could be attributed to the measurement error itself. With flight 2010 as the reference model, the parts corresponding to flight 2008 were adjusted by the algorithm of iterative closest point (ICP; Besl and McKay 1992) with specific software. For this, the 75 parts of  $2 \times 2$  km were first subdivided into another 230 smaller parts taking into account the scanner passes for flight 2008 (Fig. 6c), since in that first survey, the initial parameter data of external orientation were not fit by GCPs or some reference DEM.

To cope with the above limitations, several scripts of automation were created in PolyWorks v10 software (InnovMetric 2014) in an effort to fit each of these parts sequentially and automatically (Figs. 3 (4) and 6). The automatic process includes the incorporation of each part of the subdivision to the fit with respect to its reference model (its tile corresponding to  $2 \times 2$  km of flight 2010), and its integration again in the  $2 \times 2$  km part from which it came. With this procedure, for a sample area spanning three overlapping passes of the sensor, the exterior orientation of the flight improved, reducing the average error from  $-0.53$  to  $-0.002$  m, while the SD improved from 1.07 to 0.55 m. Also, the fit clearly improved between flights 2008 and 2010, both in mean error (from 0.179 to  $-0.022$  m) as well as in SD (from 0.87 to 0.173 m).

### Second DTM comparison

This step comprises the process of comparing new corrected DTM raster datasets (steps 1 to 3) on Fig. 3 resulting in a second DTMoD, for which the noise was reduced and the values were previously classified (Fig. 3 (5)). This enabled a review of the objects and other artifacts detected. In addition to the improvement in the orientation of flight 2008, the errors observed in the overlap areas of scanned bands almost disappeared. However, the greater noise remained in areas of strong slopes and to a lesser degree in areas with dense vegetation according to what was revealed by profiles or maps (Figs. 4d and 5d). This is related to the typical problem

**Table 1** Interpolator error expressed as the mean (absolute values) and standard deviation

Interpolator	Raster residues		Cross validation	
	Mean (m)	SD (m)	Mean (m)	SD (m)
Geostatistical reclassification	1.16	1.56	–	–
Ordinary kriging	1.14	1.62	0.91	1.52
Simply kriging	1.18	1.53	1.84	1.93
IDW	1.11	1.68	0.87	1.53

SD standard deviation, IDW inverse distance weighted



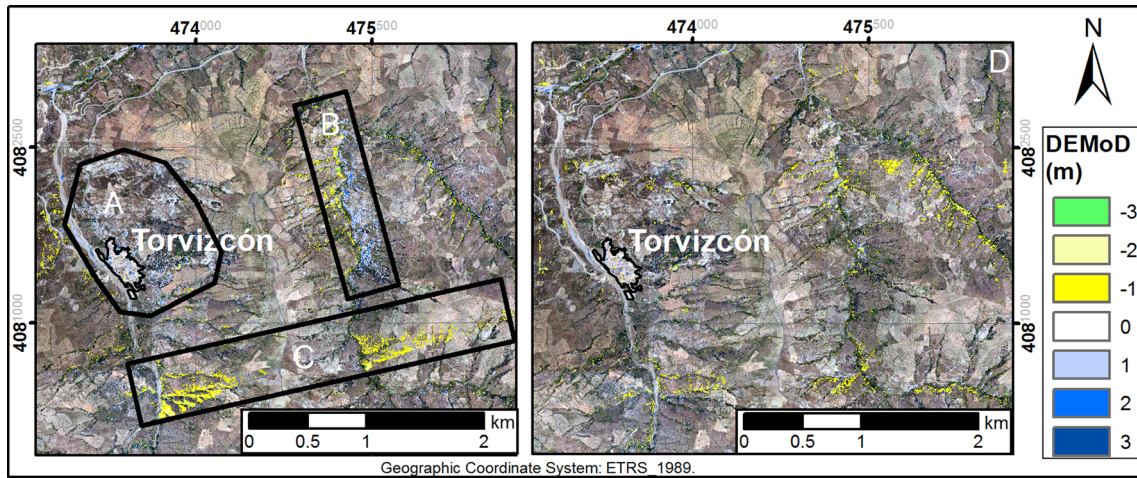


**Fig. 5** Misclassification errors in zones A (urban area), B (steep slope), and C (seam-bands). D represents the second comparison after the adjustment of the strips crossing each tile showing a considerable decreasing error in zones A, B, and C. The errors are revealed by the first DEMoD (DTMoD)

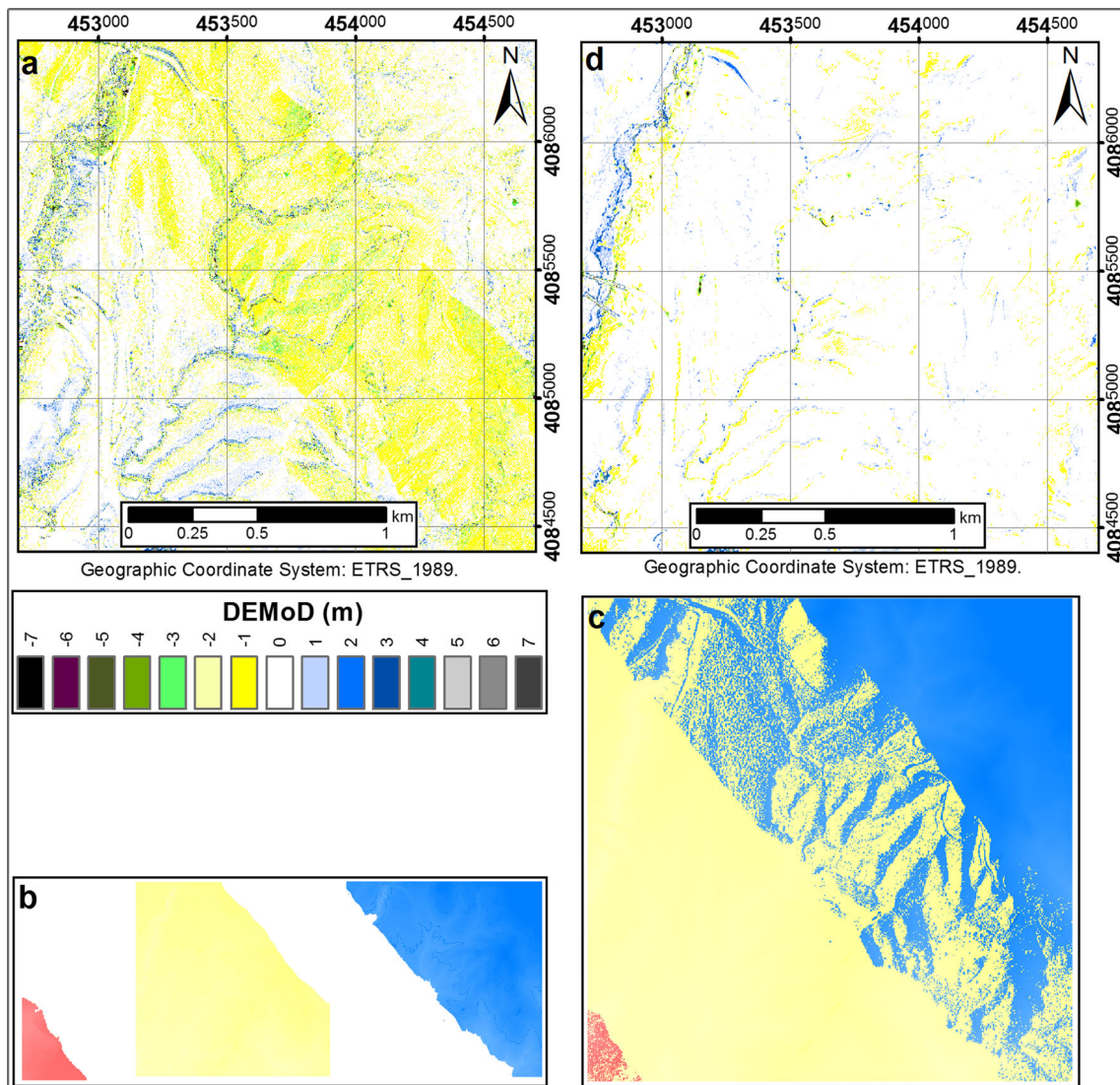


**Fig. 6** The DEMoD (DTMoD) in a represents a sample tile with initial misalignment error which fits the flight lines pattern shown in b and c (overlapped)



mentioned above and the main challenge in the investigation of LiDAR data when an effort is made to extract ground control points. When the extraction of ground control points by filtering fails, it results in points classified as ground when this is false (data-commission error), or classified as an object other than the ground when it was in fact ground (omission error), provoking an excess or shortage of points in some DTM areas located.

#### DSM comparison, generation of combined DEMoD, and delineation of the features detected

In view of the errors that arose in selecting the points classified as ground, a repeat of the process was tried in one part of the data corresponding to the digital surface model (DSM), for which the points of the first rebound of the beam were used directly without applying any classification or filtering method. In this way, it was observed that, while the differences in DSMs between the two dates presented a generalized error greater than the differences in DEM in the forest zones, due to the irregularity of these surfaces, the contrary occurred in the zones of more abrupt topography and with little vegetation (mountain crests, rocky outcrops, buildings, bridges, etc.), due to the application of the classification filters of the points clouds to generate the DTM, which can give different results in the same area depending on the coordinates of the input points incorporated in the algorithm (Fig. 3 (6)).

With this consideration, the same procedures were applied to the points from the first rebounds as to the points classified as ground in GIS, resulting in the raster representation of the highest surface over the soil (DSM) for the data of each date. In the same way, a second DEMoD was calculated (in reality this should be called DSMoD). With these new results, a new combined DEMoD was formulated automatically by selecting the value of the difference corresponding to the least absolute value found between the two differential maps (differentials of DSMs or DTMs), leading to a map of differences or DEMoD with a lower error, since in the wooded areas the DTMoD was adopted and in the abrupt topography the DSMoD (Figs. 2 (8) and 6), considering the above.

After the noise was minimized with the same geostatistical filter used in the previous cases (Fig. 3 (9)), the study area was examined visually to identify and delimit the features related to landslide phenomena according to their morphological characteristics (Fig. 3 (10)). However, in this review, three difference maps were used. That is, the last combined DEMoD was used as the best overall solution, while the DTMoD was more satisfactory in the areas with more vegetation, and the DSMoD was best to distinguish the features in places with angular or abrupt topography with less vegetation. For confirmation of the object and type of movement detected, other two kinds of layers were used, the shaded relief models to each date, and the existing orthophotography imagery for the study years with a ground sampling distance (GSD) of 0.5 m by linking them from the public web map server REDIAM (BOJA 2007) in the GIS. These information layers used to control and map the features found were adequate for most of the territory, but its resolution, despite being rather high, presented some limitations in very narrow and small areas such as steep slopes or ridges, where it became difficult to recognize the landslide processes. In addition to their little dimensions, this type of topography made it difficult to distinguish with certainty whether the changes corresponded to alterations of the terrain or simply to common errors of classification and interpolation in these areas, so that any retreat of cliffs or deposits of fallen rocks that occupy narrow elongated areas were omitted in this preliminary inventory. Except in

these areas, the shaded relief and orthophotography layers helped to resolve the uncertainty between the assignment of truly natural changes in the land, anthropic changes, or the existence of the errors mentioned above. The distinction of the landslides against other changes in the terrain (rainfall erosion, fluvial transport, anthropic alterations, or simply methodological errors) is facilitated when the depletion area and the debris deposit or displaced mass as a whole are very close to one another. Given that the negative values of DEMoD correspond to degraded areas in which the ground surface descends and the positive values correspond to accumulation areas in which the elevation of the terrain rises, they are reclassified in positive and negative values (two types) so that the source and accumulation zones for which area and volume were later calculated stand out clearly. In addition, some field campaigns have been carried out with in order to check natural landslides (Fig. 8 (a)), as well as the Google Street View selected on Google Earth locations allowed to easily check the characteristics of the slope-cut failures (Photo 1 and Photo 2 on Fig. 9).

Therefore, when the landscape features are mapped according to their dimensional or morphological characteristics and regarding the above considerations (narrow erosion escarp or deposit, accumulation separated from its origin area, etc.), the types of landslide were simplified as follows: incipient landslide, debris flow, earth flow, complex slides, and translational slides. And for the interpretation of the visual recognition, the known criteria of Hutchinson (1988), Varnes (1978), and Wieczorek (1983) were applied as described in the following:

- First, when the doubt on artificial or natural change appears, the visual checking on the orthophoto aids to distinguish between both.
- If the classified closed form have only a color corresponding to the lower values ( $-0.5$  or  $0.5$ ) and the shaded relief are also not clear, the two orthophotos corresponding to both years can be reviewed to check if a fresh, eroded, or denuded area does appears in the last later photo.
- For translational slides, a confined displaced mass almost undeformed bounded by a more or less discrete failure surfaces with a slight head rotation were observed.
- For debris flows longitudinal spread of a deformed mass were easily observed, in most cases disconnected far from the source area. This type of landslide is associated with steep gullies, and the mass is channeled to its final fan.
- Earth flows are found in less steep areas with minimum settlement in its head and surface more elongated than a translational landslide but with little deformation.
- Complex slides are assigned when a combination or a better transformation of the kind of movement was observed, for instance, when a wide scarp was observed while the mass is elongated and disconnected from its source, so it is not easy to assign the movement to a debris slide or to a debris flow.
- Incipient was assigned to those movement where only a settling (or not well-marked escarpment) without an accumulation area is observed.

#### Results and discussion

The first product from this methodology was a new detailed seasonal inventory at local scale ( $234 \text{ km}^2$ ) derived from the generation of HRDEMs registered in a geodatabase (Figs. 7, 8,

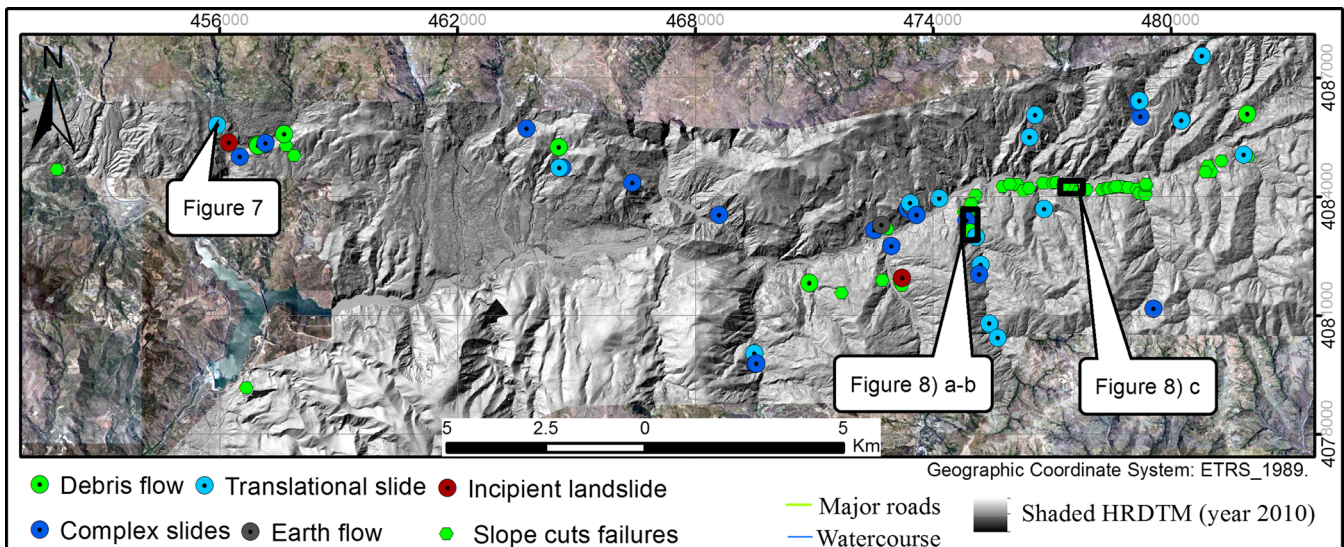


**Fig. 7** Landslide inventory map with symbolized landslide types. *Labels* indicate the location of the sample zones magnified in Figs. 8 and 9

and 9) for the period between the acquisition dates (November 2008 and July 2010). The high resolution of the DEMoD together with the HRDEMs and the orthophotography imagery allowed the inventory at local scale. Nonetheless, difficulties can be found if the aim is to address a site-specific study, when escarpments, tension crack, and other features of several meters size, or little deformation (centimeter to decimeter) should be digitized. Furthermore, the statistical process of noise reduction and classification limits the range of detection to changes greater than 0.5 m in absolute value, including them into classes 1 and -1, respectively. On the other hand, an imprecision does exist when establishing the duration of such changes or displacements, as the date of the initiation of the failure or reactivation and its completion are unknown data. Nevertheless, an approximation of the minimum velocity has been estimated taking into account the time window between the two data acquisitions ( $\approx 20$  months) together with the minimum absolute displacement detected (0.5 m), so the value obtained is 0.025 m/month (0.3 m/year), and considering the classification of (Cruden and Varnes 1996) these velocities correspond to very low landslides (16 mm/year–1.6 m/year), but this does not apply to debris flow or rapid translational landslides for instance.

Respecting the production time, without taking into account the days necessary planning the flights, capturing the data and preparing them, once the methodology was ready to apply it, the approximate time to obtain the final map is about 5 days to the study area (including the semi-automatic adjustment of raw data), being the longest task the visual recognition and digitizing of the landslides and slope-cut failures taking 4 days. Several hours can be saved if the raw data are well adjusted depending on the computer equipment available. For this work was used a computer mounted with an Intel® Core™ i7-3820 CPU @ 3.60 GHz, 24 GB RAM, Graphic card GeForce GTX 285 (1 GB DDR) and a 64 bits OS. Thus comparing this with the reviewed methods in Guzzetti et al. (2012), this methodology provides an effective alternative.

The final inventory map consists of two separate layers (see Fig. 7) registered in a geodatabase, one containing 47 natural landslides and other containing 50 slope-cut failures. Although

the exact date is not known, they were assigned to the period between the two acquisitions dates; however, they are thought as a consequence of the exceptional from October 2009 to March 2010. In the case of the natural landslides, they were classified into 25 debris slides, 17 complex slides, 3 earth flows, and 2 incipient slides; while in the case of the slope-cut failures, all of them presented characteristics of translational slides with nearly no deformation in its displacement.

After the inventory was completed, the natural landslides identified, the areas, and number of spatial intersections between each movement and the layers of susceptibility and lithology (DIPGRA/IGME 2007) were calculated using different GIS tools. This is an approach to analyze the spatial distribution of the new inventory regarding the lithology and the susceptibility zoning existing in the area, but this is not intended to validate the susceptibility map from the inventory, as the susceptibility map has been assessed using an inventory with different ages while the new inventory only includes the events happened in less than 2 years. On the other hand, the difficulties to check or validate all the inventoried landslides and the completeness of the own inventory appear principally in inspecting the entire area looking for non-inventoried landslides, or in knowing if other little landslides were removed by the runoff water; however, some campaigns of field work were carried out to check some of the more accessible landslides (Fig. 7a).

From this assessment, certain useful spatial relations were discovered. The first noteworthy results show a greater area affected when combining the translational slide type and phyllites with intercalated calcareous rocks (69.8 %) and then, over quartzites and quartzite schists (15.16 %), while the conglomerates, calcareous crust, and travertines were almost unaffected by the different types of movement (Tables 2 and 3 and Fig. 10). Nevertheless, given the frequency of the landslides detected from their representative points, the number of them together with the phyllite, quartzite, and quartzite schist were almost the same (40 %), followed by calcareous rocks (limestones, dolomites, calcschists) with 17 % of the failures (Table 2). In general, the area covered by phyllites was the most affected one, with the greater size of the



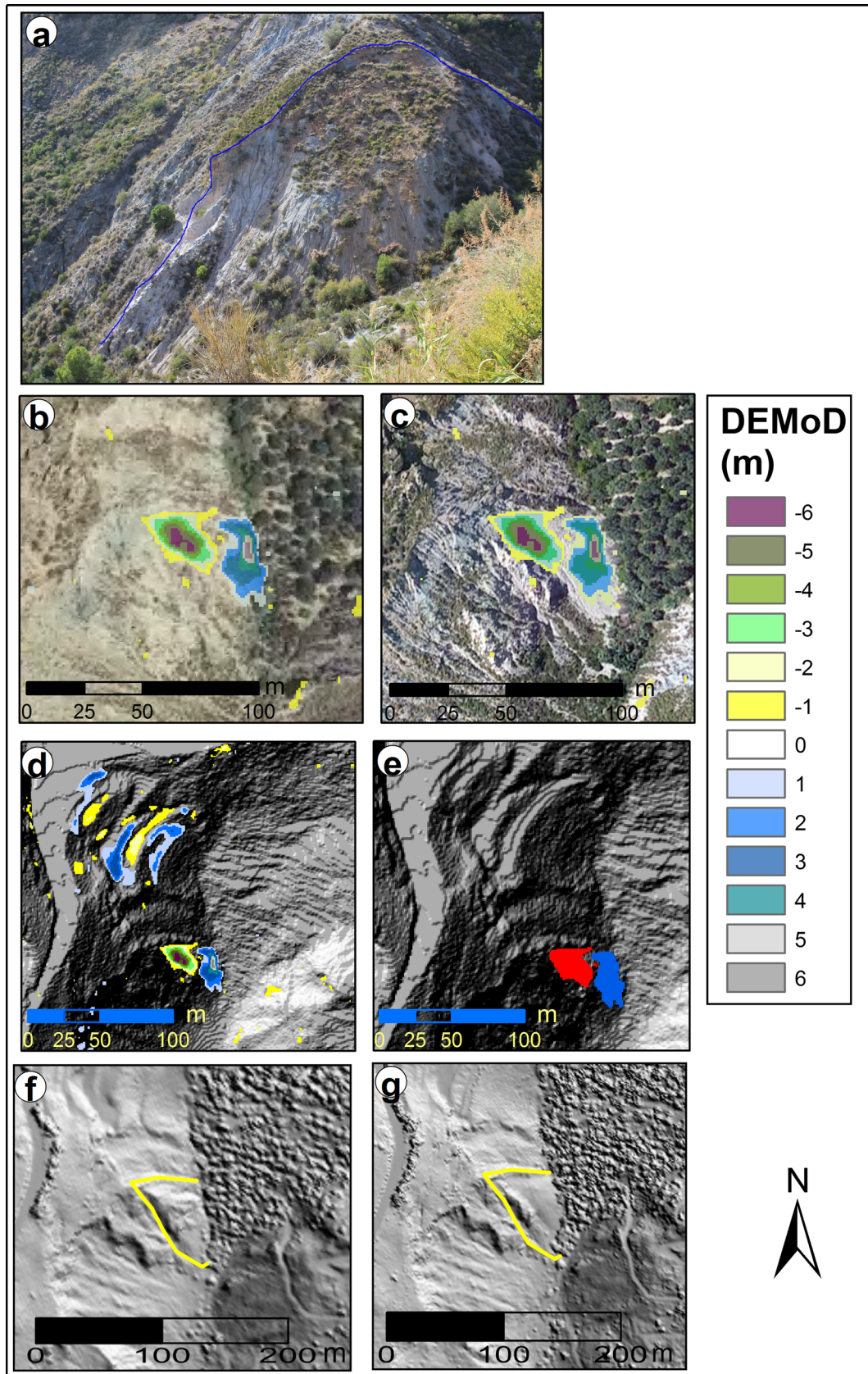


**Fig. 8** Translational slide labelled in Fig. 7. **a** Field photography of the landslide. **b** and **c** show the superimposed combined DEM<sub>o</sub>D to the orthophotos of years 2007 and 2010, respectively. In **d**, the DEM<sub>o</sub>D overlays the *shaded relief* (DTM of the year 2010) showing the artificial earth works and the landslides whose settled head (*red*) and mass (*blue*) are distinguished in **e**. **f** and **g** show the *shaded relief* based on the DSMs of 2008 and 2010, respectively, as well as the delimited landslide mass before and after the failure



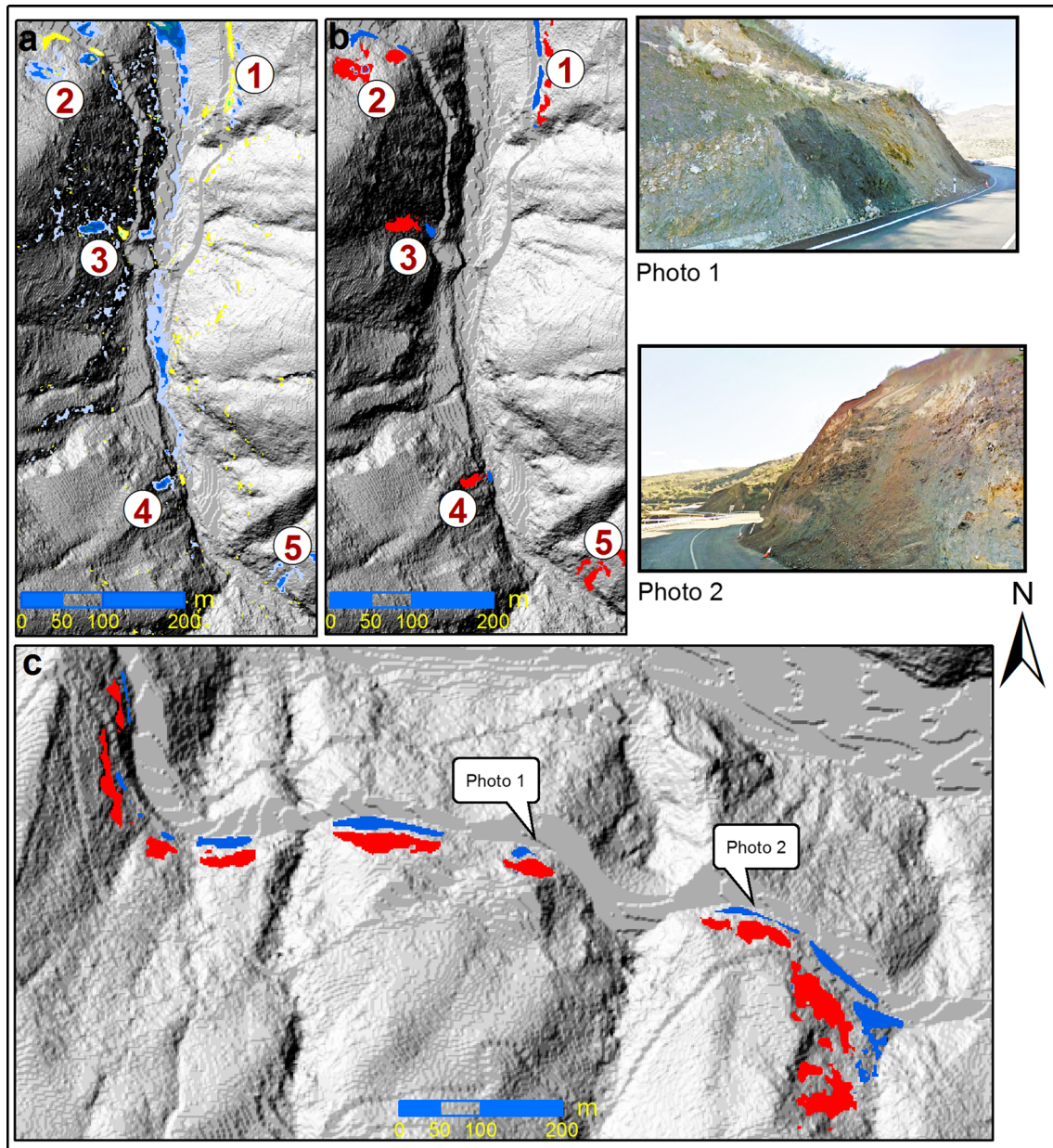


**Fig. 9** a Part a, located in Fig. 7, shows the shaded relief (year 2010) and the overlaid combined DEMoD where several landslides and slope-cut failures were mapped. The same features are presented in b showing downward (red) and upward (blue) general senses of movements. Numbers 1 and 2 are referred to slope-cut failures, while 3 to 5 are referred to natural landslides. In the same way, c shows a sample of slope-cut failures along a stretch of road also located in Fig. 7. As a check, photos 1 and 2 show evidences on the slope cuts indicated in c

translational slides developed in these areas, while in other lithologies such as the quartzitic schists, the observed translational slides were of smaller size. The alluvial deposits and debris deposits were less affected by this type of phenomenon, although they could be probably more affected by erosion (this being beyond the scope of the present study). The smallest area affected in the rocks where the predominant slope movement was translational sliding (conglomerate limestone, dolomite, calcareous crust, and travertines) can be attributed to the higher quality and strength of these more massive and less blocky rock massifs.

When the inventory layer was crossed with the susceptibility map, two important distinctions were made. First, the areas of moderate susceptibility class were visibly affected by more than

double the area (69,766 m<sup>2</sup>) with respect to high susceptibility (32,544 m<sup>2</sup>; Table 4 and Fig. 11), although a lesser degree was found on comparing the percentage of movements in each type of susceptibility (57.47 vs. 42.55 %, taking into account the frequency of their representative points, respectively). However, special care must be taken when interpreting these results for the following reasons; on the one hand, it does exist a significant difference between the time window covered by this recent seasonal inventory and the multi-temporal one used to assess the susceptibility zoning what include events from remote times to more recent periods (historical). On the other hand, the change to which the main determining factors are submitted with time should be considered (climatology, slope gradient, etc.). These

**Table 2** Landsliding affected area (source+accumulation) and count (representative points) by lithology

Lithology	Affected area (%)	Representative points (%)
Calcareous crust and travertine	0.08	–
Conglomerate	2.43	4.26
Aluvial and debris deposits	3.73	–
Limestone, dolostone, and calc-schist	8.78	17.02
Quartzite and quartzite schist	15.16	38.30
Phyllite with interbedded calcareous rocks	69.81	40.43
Total	100.00	100.00

considerations can cause the classes of greater susceptibility (moderate and high) to alternate throughout the area of interest. As a result, due to the close relation between these two highest classes, the inventory distribution can differ from predicted by the susceptibility map. Secondly, translational slides are found in all the susceptibility classes, even in lowest susceptibility class. Other patent observation is the high frequency of debris flows and complex slides with respect to other types of movements.

Among other characteristics easily recognized by this methodology (alteration of the edges of fluvial beds, anthropic changes, etc.), the stability of slope cuts also constitutes an important process that directly affect highways or other infrastructures and private property, although commonly controlled more by the quality of the design and construction than by natural factors. In this way, the slope-cut failures were also inventoried. This type of process, as opposed to the phenomena of natural slope movements, proved to be more frequent in quartzites and quartzite schists. This can be explained by the construction and modification of a large stretch of highway in the eastern part with steep slopes, where quartzite schists predominate with high susceptibility to landslides (Tables 5 and 6). On the other hand, Table 6 shows a larger area covered by these in moderate susceptibility zones (66.43 %), while their representative points of these failures are more frequent in the high-susceptibility class (58 %).

The inventory covers the special wet period from October 2009 to March 2010, during which the cumulative precipitation for two

**Table 3** Landsliding affected area (source+accumulation) and count (centroids) by lithology

Landslide type	Affected area (%)	Affected area ( $\times 100 \text{ m}^2$ )
Incipient landslide	1.73	18.07
Debris flow	4.81	50.22
Earth flow	6.56	68.45
Complex slide	15.01	156.64
Translational slide	71.88	749.92
Total	100.00	1043.29

representative pluviometric stations was 247 % (Torvizcón station) and 221 % (Órgiva station) with respect to the average for that months, corresponding to quantities measured of 485 and 782 mm, respectively (Irigaray and Palenzuela 2013). Thus, the majority of the landslides inventoried can be attributed to that rainfall as the triggering factor.

### Conclusions

The present work develops a new methodology for mapping landslides, based on the use of advanced LiDAR with GIS technology. This approach has provided a way of compiling inventories in less time, specifically in less than one week, overcoming some old problems (difficult access, uncertainty of subjectivity) that hamper mapping georeferenced features with greater precision in a more effective way. And regarding the increasing of public orthophotography imagery and LiDAR data production, this methodology comprises a manner of keeping the geodatabases updated or mapping a timely post-event inventory.

The preliminary results using this methodology come from the processing of HRDEMs, automating certain tasks by scripts and models of user-friendly GIS tools where needed in order to identify and delineate the potentially unstable DEMoD areas that were integrated into the geospatial database together with other attributes. Thus, the landslides were delineated in a short time after all the data processing was applied in a semi-automatic way and supervised, giving rise to the seasonal inventory between the dates programmed for the acquisition. These inventories are constructed in a more objective and complete way than when being handled by a group of experts through field work and a conventional office over several weeks or months (field mapping, even using DGPS, photointerpretation, etc.). The most time-consuming process in this methodology is the visual reviewing and then the realignment and the filtering of LiDAR data. To accelerate the latter task in the present work, the fit based on the ICP between corresponding parts of the data of both flights was made sequentially and semi-automatically over all of them. Nevertheless, this fit can be omitted when the quality of the data gathered is greater, that is, when the overlapping bands between scanner passes have a minimum error that can be attributed to the measurement equipment, as in the case of flight 2010 used as a reference. Regarding the automatic classification by filtering the LiDAR data to distinguish between ground points and non-ground points, the process is conducted in only a few hours or even less, depending on the computer equipment used. Other subsequent processing procedures such as the edition of the models are not necessary in this work, in which the measurements were made directly over the land and require only a preliminary qualitative calculation of vertical movements, which also implies a major time savings.

The methodology is recommended to digitally map landslides and even features (i.e., major escarpments, lateral escarpments, toe border or slope break) from local scale to minor scales (regional, national) detecting the changes highlighted and isolated by the DEMoD. When trying to collect some features groups of classified pixels can appear that do not clearly define the morphology of a landslide and need to be confirmed by auxiliary layers such as the orthoimages or shaded relief layers with high resolution used in this case. Under the assumption of all this, the characteristics of the products generated can even surpass the recommended scale (1:15,000) for the detection of small- or medium-sized movements

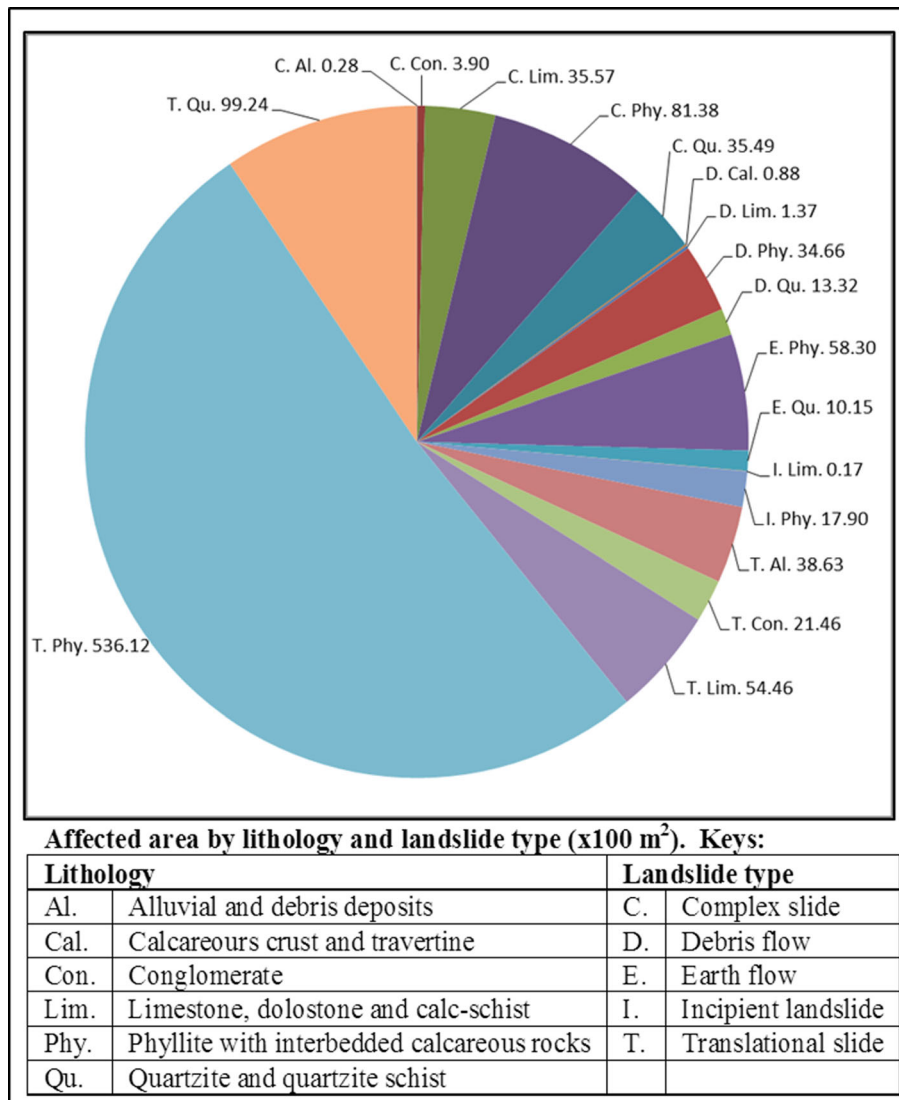


**Fig. 10** Affected area by landslide type and lithology

(Mantovani et al. 1996), although smaller features (little secondary escarpments, tension cracks, or little displacements) are not so evident in the results of this methodology. Nonetheless, this local-seasonal inventory can be used as a starting point to planners or researchers to determine zones where landslides are spatially more

frequently, as well as to reveal new landslide failures or previously unknown ones which can now be selected to be monitored by higher-resolution techniques (TLS, high-resolution digital photogrammetry or the edition of DEMs LiDAR with the support of stereoscopic models) to reveal smaller features and displacements.

**Table 4** Landsliding affected area and frequency (representative points) by susceptibility class

Susceptibility class	Affected area (%)	Affected area (x100 m <sup>2</sup> )	Representative points (%)
Low	0.79	8.28	–
Very low	1.14	11.91	–
High	31.19	325.44	42.55
Moderate	66.87	697.66	57.45
Total	100.00	1043.29	100.00

One limitation worth mentioning in applying this type of methodology is the common effect of omitting parts of the landscape caused in some areas by the semi-automatic or automatic extraction of points of land when applying the data filtering or classification. This effect was counteracted in good part by the combination of the two maps of differences, DTMoD and DSMoD, although some of the most abrupt areas remained where the fall of rocks or collapses of small size could not be differentiated, since the beveling brought about by these effects could be misinterpreted as one of these movements.

This reflects not only the importance of the resolution of the data, which depends directly on the height of the flight and which defines the exactitude and smaller size of the features detected, but also the accurate classification of the raw data, the perfection of



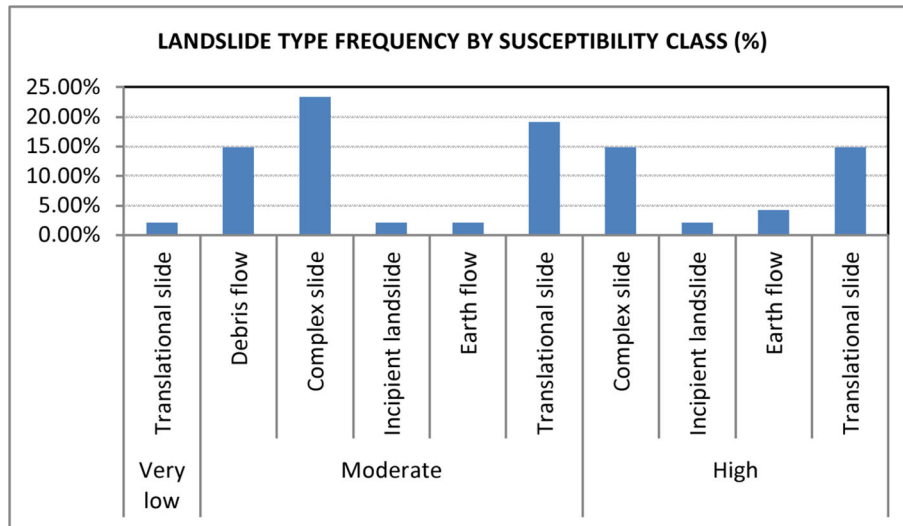


**Fig. 11** Landsliding frequency by landslide type and susceptibility class

which continues to be a challenge today. In fact, the completeness and exactness of the new inventories constructed with this methodology depend on these two factors, i.e., the resolution or density of the data acquired and the correct extraction of the ground points.

It bears emphasizing that the capacities related to this technique make it easy to bring together other characteristics (dynamic fluvial changes, changes in land use, monitoring of infrastructure construction, etc.), for which the inventory also included slope-cut failure over highways, caused by strong seasonal rains during the wet season of the hydrological year 2009–2010, delineating them in the same way as the natural movements inventoried.

With this, methodology advances have been made with the main aim of improving and streamlining the collection of events within the inventories of landslides in the most extensive areas, this constituting the basis for calculating the frequency of these events and for assessing their true hazard. On the other hand, a preliminary comparison between the new areal distribution of landsliding frequency and the zones classified by the susceptibility map was carried out. According to the results, the area and number of landslides found in the moderate susceptibility zone were higher than for the high-susceptibility zone, 66.87 % in moderate susceptibility zones as opposed to 31.19 % in the high-

susceptibility ones regarding their occupied area, or 57.45 % in moderate susceptibility zones vs. 42.55 % in the high-susceptibility ones regarding their frequency (Table 4). However, it should be noted that the difference in temporal scale between the new seasonal inventory, just compiled according to the changes that occurred after a period of significant rains (which possibly triggered most of these events), with respect to the scale of the inventory used to generate the susceptibility map, as well as the possible changes in the determining factors, influences the degree of the relation between the predicted relative density by susceptibility assessment and the distribution assigned by the real inventory. This suggests that successive inventories made by using this or other techniques can increase the information to achieve a more reliable correlation with susceptibility maps calculated from inventories at broader temporal scale and to allow a better calibration on the initial susceptibility model. Furthermore, if the update of these geodatabase is conducted frequently, it will supply more accuracy and complete inventory to assess the quantitative landslide hazard.

Is important to refer here the atypical cumulated rain from October 2009 to March 2010 (both inclusive) measured in two representative stations in the study area what overcome historical record, by which possibly these rains are the triggering for most of the landslides and slope-cut failures as consequence of the high pore pressure reached because of the infiltration. Nonetheless, further investigation is necessary to approach the date of the probably landsliding initiation or completion, and thus the

**Table 5** Slope-cut failure affected area and frequency by lithology

Lithology	Affected area (%)	Representative points (%)
Conglomerate	–	–
Phyllite with interbedded calcareous rocks	7.31	16.33
Limestone, dolostone and calc-schist	7.88	4.08
Quartzite and quartzite schist	84.80	79.59
Total general	100.00	100.00

**Table 6** Slope-cut failure affected area and frequency (representative points) by susceptibility class

Susceptibility class	Affected area (%)	Representative points (%)
Moderate	66.43	42.00
High	33.57	58.00
Total general	100.00	100.00

threshold of the triggering rainfall or the velocity associated with those movements.

### Acknowledgments

This research was supported by projects CGL2005-03332 and CGL2008-04854 funded by the Ministry of Science and Education of Spain, and Excellence Project Po6-RNM-02125, funded by the Regional Government. It was developed in the RNM121 and TEP213 Research Groups funded by the Andalusian Research Plan.

### References

- AEMET (2010) Resumen anual climatológico 2010. Agencia Estatal de Meteorología. [http://www.aemet.es/documentos/es/serviciosclimaticos/vigilancia\\_clima/resumenes\\_climat/anuales/res\\_anual\\_dim\\_2010.pdf](http://www.aemet.es/documentos/es/serviciosclimaticos/vigilancia_clima/resumenes_climat/anuales/res_anual_dim_2010.pdf)
- Ardizzone F, Cardinali M, Galli M, Guzzetti F, Reichenbach P (2007) Identification and mapping of recent rainfall-induced landslides using elevation data collected by airborne Lidar. *Nat Hazards Earth Syst Sci* 7:637–650
- Axelsson P (2000) DEM generation from laser scanner data using adaptive TIN models. *Int Arch Photogramm Remote Sens* 33:111–118
- Baum RL, Coe JA, Godt JW, Harp EL, Reid ME, Savage WZ, Schulz WH, Brien DL, Chleborad AF, McKenna JP, Michael JA (2005) Regional landslide-hazard assessment for Seattle, Washington, USA. *Landslides* 2:266–279
- Besl PJ, McKay ND (1992) A method for registration of 3-D shapes. *IEEE Trans Pattern Anal Mach Intell* 14:239–256
- BOJA (2007) Red de Información Ambiental de Andalucía (REDIAM). Consejería de Medio Ambiente y Ordenación del Territorio, Junta de Andalucía. Ley 7/2007, de 9 de julio, de Gestión Integrada de la Calidad Ambiental. Boletín Oficial de la Junta de Andalucía, 143
- Brabb EE (1984) Innovative approaches to landslide hazard and risk mapping, 4 th International Symposium on Landslides, Toronto, Canada, Vol. 1, pp 307–323
- Carrara A, Guzzetti F, Cardinali M, Reichenbach P (1999) Use of GIS technology in the prediction and monitoring of landslide hazard. *Nat Hazards* 20:117–135
- Cascini L (2008) Applicability of landslide susceptibility and hazard zoning at different scales. *Eng Geol* 102:164–177
- Cascini L, Bonnard C, Corominas J, Jibson R, Montero-Olarte J (2005) Landslide hazard and risk zoning for urban planning and development – state of the art report. In: Hungr, fell, couture, Eberhardt (eds) *Landslide risk management*. Taylor and Francis, London, pp 199–235
- Chacón J, Irigaray C, Fernandez T, El Hamdouni R (2006a) Engineering geology maps: landslides and geographical information systems. *Bull Eng Geol Environ* 65:341–411
- Chacón J, Irigaray C, Fernández T, El Hamdouni R (2006b) Landslides in the main urban areas of the Granada province, Andalucía, Spain. *IAEG 2006*, Nottingham
- Chacón J, Irigaray C, El Hamdouni R, Jiménez-Perálvarez J (2010) Diachroneity of landslides. In: Williams AL, Pinches GM, Chin CY, McMorran TJ, Massey CI (eds) *Geologically active*. Taylor & Francis Group, CRC Press-Balkema Vol. 1, pp 999–1006
- Corominas J, van Westen C, Frattini P, Cascini L, Malet JP, Fotopoulou S, Catani F, Van Den Eeckhaut M, Mavrouli O, Agliardi F, Pitilakis K, Winter MG, Pastor M, Ferlisi S, Tofani V, Hervás J, Smith JT (2014) Recommendations for the quantitative analysis of landslide risk. *Bull Eng Geol Environ* 73:209–263
- Cruden DM, Varnes DJ (1996) Landslide types and processes. Special report—National Research Council. *Transp Res Board* 247:36–75
- Daehne A, Corsini A (2013) Kinematics of active earthflows revealed by digital image correlation and DEM subtraction techniques applied to multi-temporal LiDAR data. *Earth Surf Process Landf* 38:640–654
- Derron MH, Jaboyedoff M (2010) Preface to the special issue. In: *LIDAR and DEM techniques for landslides monitoring and characterization*. *Nat Hazards Earth Syst Sci* 10:1877–1879
- Dewitte O, Jasselette JC, Cornet Y, Van Den Eeckhaut M, Collignon A, Poesen J, Demoulin A (2008) Tracking landslide displacements by multi-temporal DTMs: a combined aerial stereophotogrammetric and LIDAR approach in western Belgium. *Eng Geol* 99:11–22
- DIPGRA/IGME (2007) Atlas de Riesgos Naturales en la Provincia de Granada. Diputación de Granada / Instituto Geológico de y Minero de España, Gráficas Chile, 190 pp. ISBN: 978-84-7807-438-9
- El Hamdouni R, Irigaray C, Fernández T, Chacón J, Keller EA (2008) Assessment of relative active tectonics, southwest border of the Sierra Nevada (southern Spain). *Geomorphology* 96:150–173
- ESRI (2013) ArcGIS Desktop 10.0. Environmental Systems Research Institute, Inc (ESRI). <http://www.esri.com/>
- Evans JS, Hudak AT (2007) A multiscale curvature algorithm for classifying discrete return LiDAR in forested environments. *IEEE Trans Geosci Remote Sens* 45:1029–1038
- Fell R, Corominas J, Bonnard C, Cascini L, Leroi E, Savage WZ (2008) Guidelines for landslide susceptibility, hazard and risk zoning for land use planning. *Eng Geol* 102:85–98
- Fernández T, Irigaray C, El Hamdouni R, Chacón J (2003) Methodology for the assessment of slope susceptibility and mapping by means of a GIS. Application to the Contraviesa area (Granada, Spain). *Nat Hazards* 30:297–308
- Fernández T, Jiménez-Perálvarez JD, Fernández P, El Hamdouni R, Cardenal FJ, Delgado J, Irigaray C, Chacón J (2008) Automatic detection of landslide features with remote sensing techniques in the Betic Cordilleras (Granada, Southern Spain). *The International Archives of the Photogrammetry, Remote Sensing and Spatial Information Sciences*, XXXVII. Part B8: 351–356. ISSN: 1682–1750
- Fernández P, Irigaray C, Jimenez J, El Hamdouni R, Crossetto M, Monserrat O, Chacon J (2009) First delimitation of areas affected by ground deformations in the Guadalfeo River Valley and Granada metropolitan area (Spain) using the DInSAR technique. *Eng Geol* 105:84–101
- Fernández T, Pérez J, Delgado J, Cardenal F, Irigaray C, Chacón J (2011) Evolution of a diachronic landslide by comparison between different DEMs obtained from Digital Photogrammetry Techniques in Las Alpujarras (Granada, Southern Spain). *Conference of Geoinformation for Disaster Management (GI4DM)*. Antalya, Turkey
- Fernández T, Jiménez J, Delgado J, Cardenal J, Pérez JL, El Hamdouni R, Irigaray C, Chacón J et al (2013) Methodology for landslide susceptibility and hazard mapping using GIS and SDI. In: Zlatanova S (ed) *Intelligent systems for crisis management, lecture notes in geoinformation and cartography*. Springer-Verlag, Berlin. doi:10.1007/978-3-642-33218-0\_14
- Galli M, Ardizzone F, Cardinali M, Guzzetti F, Reichenbach P (2008) Comparing landslide inventory maps. *Geomorphology* 94:268–289
- Glenn NF, Streutker DR, Chadwick DJ, Thackray GD, Dorsch SJ (2006) Analysis of LiDAR-derived topographic information for characterizing and differentiating landslide morphology and activity. *Geomorphology* 73:131–148
- Gómez-Pugnaire MT, Galindo-Zaldívar J, Rubatto D, González-Lodeiro F, López Sánchez-Vizcaino V, Jabaloy A (2004) A reinterpretation of the Nevado-Filábride and Alpujarride complexes (Betic Cordillera): field, petrography and U-Pb ages from orthogneisses (western Sierra Nevada, S Spain). *Schweiz Miner Petrogr Mitt* 84:303–322
- Guzzetti F, Mondini AC, Cardinali M, Fiorucci F, Santangelo M, Chang KT (2012) Landslide inventory maps: new tools for an old problem. *Earth Sci Rev* 112:42–66
- Haneberg WC, Cole WF, Kasali G (2009) High-resolution lidar-based landslide hazard mapping and modeling, UCSF Parnassus Campus, San Francisco, USA. *Bull Eng Geol Environ* 68:263–276
- Hervás J, Barredo JJ, Rosin PL, Pasuto A, Mantovani F, Silvano S (2003) Monitoring landslides from optical remotely sensed imagery: the case history of Tessina landslide, Italy. *Geomorphology* 54:63–75
- Hutchinson JN (1988) General report: morphological and geotechnical parameters of landslides in relation to geology and hydrogeology. *Landslides. Proc. 5th symposium*, Lausanne, 1988 1:3–35
- Ibsen ML, Brunsden D (1996) The nature, use and problems of historical archives for the temporal occurrence of landslides, with specific reference to the south coast of Britain, Ventnor, Isle of Wight. *Geomorphology* 15:241–258
- InnovMetric (2014) PolyWorks. InnovMetric Software Inc. <http://www.innovmetric.com/>
- Irigaray C, Palenzuela JA (2013) Análisis de la actividad de movimientos de ladera mediante láser escáner terrestre en el suroeste de la Cordillera Bética (España). *Rev Geol Apl Ing Ambient* 31:53–67
- Irigaray C, Fernández T, El Hamdouni R, Chacón J (1999) Verification of landslide susceptibility mapping: a case study. Technical report. *Earth Surf Process Landf* 24:537–544
- Irigaray C, Lamas F, El Hamdouni R, Fernandez T, Chacon J (2000) The importance of the precipitation and the susceptibility of the slopes for the triggering of landslides along the roads. *Nat Hazards* 21:65–81

- Irigaray C, Fernández T, El Hamdouni R, Chacón J (2007) Evaluation and validation of landslide-susceptibility maps obtained by a GIS matrix method: examples from the Betic Cordillera (southern Spain). *Nat Hazards* 41:61–79
- Isenburg M (2013) LAStools - efficient tools for LiDAR processing. Version 130506. <http://www.cs.unc.edu/~isenburg/lastools/>
- Jaboyedoff M, Oppikofer T, Abellán A, Derron M-H, Loye A, Metzger R, Pedrazzini A (2012) Use of LiDAR in landslide investigations: a review. *Nat Hazards* 61:5–28
- Jimenez-Perálvarez JD, Irigaray C, El Hamdouni R, Chacon J (2009) Building models for automatic landslide-susceptibility analysis, mapping and validation in ArcGIS. *Nat Hazards* 50:571–590
- Jiménez-Perálvarez JD, Irigaray C, El Hamdouni R, Chacón J (2011) Landslide-susceptibility mapping in a semi-arid mountain environment: an example from the southern slopes of Sierra Nevada (Granada, Spain). *Bull Eng Geol Environ* 70:265–277
- Kasai M, Ikeda M, Asahina T, Fujisawa K (2009) LiDAR-derived DEM evaluation of deep-seated landslides in a steep and rocky region of Japan. *Geomorphology* 113:57–69
- Leica (2006) Leica Geosystems presents its Leica ALS50-II LiDAR System: higher accuracy with pulse rates up to 150 kHz. [http://www.leica-geosystems.com/en/About-us-News\\_360.htm?id=1250](http://www.leica-geosystems.com/en/About-us-News_360.htm?id=1250)
- Mantovani F, Soeters R, Van Westen CJ (1996) Remote sensing techniques for landslide studies and hazard zonation in Europe. *Geomorphology* 15:213–225
- Marsella M, Proietti C, Sonnessa A, Coltelli M, Tommasi P, Bernardo E (2009) The evolution of the Sciarra del Fuoco subaerial slope during the 2007 Stromboli eruption: relation between deformation processes and effusive activity. *J Volcanol Geotherm Res* 182:201–213
- McKean J, Roering J (2004) Objective landslide detection and surface morphology mapping using high-resolution airborne laser altimetry. *Geomorphology* 57:331–351
- Meng X, Currit N, Zhao K (2010) Ground filtering algorithms for airborne LiDAR data: a review of critical issues. *Remote Sens* 2:833–860
- Palenzuela JA, Irigaray C, Jiménez-Perálvarez JD, Chacón J (2013) Application of terrestrial laser scanner to the assessment of the evolution of diachronic landslides. In: Margottini C, Canuti P, Sassa K (eds) *Landslide science and practice vol. 2*, 517–523. Springer, Berlin. ISBN 978-3-642-31445-2
- Prokešová R, Kardoš M, Medved'ová A (2010) Landslide dynamics from high-resolution aerial photographs: a case study from the Western Carpathians, Slovakia. *Geomorphology* 115:90–101
- Prokop A, Panholzer H (2009) Assessing the capability of terrestrial laser scanning for monitoring slow moving landslides. *Nat Hazards Earth Syst Sci* 9:1921–1928
- Roering JJ, Mackey BH, Marshall JA, Sweeney KE, Deligne NI, Booth AM, Handwerker AL, Cerovski-Darriau C (2013) You are HERE: connecting the dots with airborne lidar for geomorphic fieldwork. *Geomorphology* 200:172–183
- Singhroy V, Molch K (2004) Characterizing and monitoring rockslides from SAR techniques. *Adv Space Res* 33:290–295
- Soeters R, van Westen CJ (1996) Slope instability recognition, analysis and zonation. In: Turner S (ed) *Landslides investigation and mitigation*. TRB special report 247. National Academy Press, Washington D.C., pp 129–177
- Tarolli P, Sofia G, Dalla Fontana G (2012) Geomorphic features extraction from high-resolution topography: landslide crowns and bank erosion. *Nat Hazards* 61:65–83
- Van Den Eeckhaut M, Hervás J (2012) State of the art of national landslide databases in Europe and their potential for assessing landslide susceptibility, hazard and risk. *Geomorphology* 139–140:545–558
- van Westen CJ, van Asch TWJ, Soeters R (2006) Landslide hazard and risk zonation—Why is it still so difficult? *Bull Eng Geol Environ* 65:167–184
- van Westen CJ, Castellanos E, Kuriakose SL (2008) Spatial data for landslide susceptibility, hazard, and vulnerability assessment: an overview. *Eng Geol* 102:112–131
- Varnes DJ (1978) Slope movement types and processes. In: Schuster K (ed) *Landslides: analysis and control*, vol 176. TRB, National Research Council, Washington D.C., Vol.: Special Report, pp 11–33
- Varnes DJ (1984) Landslide hazard zonation: a review of principles and practice, Commission on landslides of IAEG, UNESCO, Paris. *Natural Hazards*, Vol 3
- Wang G, Joyce J, Phillips D, Shrestha R, Carter W (2013) Delineating and defining the boundaries of an active landslide in the rainforest of Puerto Rico using a combination of airborne and terrestrial LiDAR data. *Landslides* 10(4):503–513
- Wieczorek GF (1983) Preparing a detailed landslide-inventory map for hazard evaluation and reduction. *Bull Assoc Eng Geol* 21:337–342
- Zhang K, Chen S-C, Whitman D, Shyu M-L, Yan J, Zhang C (2003) A progressive morphological filter for removing nonground measurements from airborne LiDAR data. *Geosci Remote Sens IEEE Trans* 41:872–882

**J. A. Palenzuela · J. Chacón · C. Irigaray** (✉)

Department of Civil Engineering,  
University of Granada,  
Granada, Spain  
e-mail: clemente@ugr.es

**M. Marsella · C. Nardinocchi**

Dip. Ingegneria Civile, Edile, Ambientale,  
Università "La Sapienza",  
Rome, Italy

**J. L. Pérez · T. Fernández**

Department of Cartographic, Geodetic and Photogrammetric Engineering,  
University of Jaén,  
Jaén, Spain